An Analytical Model Integrated with Toolpath Design for Wrinkling Prediction in Conventional Spinning

Z. H. Li and H. Long*

Department of Mechanical Engineering, the University of Sheffield, Sheffield, UK

* Corresponding author, email address: h.long@sheffield.ac.uk

Abstract

Blank wrinkling is the most frequently encountered material processing failure in spinning. Design of toolpath profiles and selection of process parameters are important in preventing wrinkling. Existing studies employ simplified toolpath profiles and rely on the calculation of maximum and critical stresses of the blank to determine the onset of wrinkling, often requiring time-consuming Finite Element simulations. To overcome these limitations, this paper develops an analytical wrinkling prediction model integrated with toolpath design in developing multi-pass conventional spinning. The toolpath design is parameterised for concave, convex and linear profiles and a wrinkling-wave function using a concave profile is developed to capture geometrical characteristics of a wrinkled blank. The forming depth is introduced as a critical variable in designing a toolpath profile to control wrinkling. Material plastic deformation is analysed by employing the Donnell-Mushtari-Vlasov theory and wrinkling initiation is predicted by the occurrence of the instability of the blank as a doubly-curved thin shell. Experimental tests of first-pass conventional spinning using concave, convex and linear toolpath profiles are performed to validate the developed wrinkling prediction model. The experimental validation confirms that the proposed critical forming depth of toolpath profile is an accurate and effective measure in predicting the onset of wrinkling. The results show the significant effect of the design of toolpath profile, blank thickness, spin ratio and feed ratio on the onset of the wrinkling. The wrinkling prediction model is capable of producing processing maps of these key parameters to prevent wrinkling for the spinning process development in practical applications.

Keywords: Conventional spinning; Wrinkling; Processing map.

1. Introduction

Sheet metal spinning is one of the oldest known metal forming processes. With the growing demand for lightweight engineering components in recent times, the sheet metal spinning has been increasingly applied in manufacturing products for many industrial applications. The sheet metal spinning can be divided into conventional spinning and shear spinning. The conventional spinning process is commonly used to produce axisymmetric products by using a roller tool. Multi-passes are required for the roller tool to progressively deform a flat metal blank onto a spinning mandrel to produce a desired geometry with an aim to keep the blank thickness unchanged after the spinning process. Due to localised material plastic deformation, the conventional spinning has inherent advantages, such as low forming force, good dimensional accuracy, high material utilisation, and enhanced mechanical properties of the blank material after spinning. One of the important advantages is that no special tools or dies are required thus the spinning process can flexibly manufacture various geometries and materials cost effectively. The process design of a conventional spinning process includes decisions on the number of roller tool passes, toolpath profiles, and spinning process parameters. These depend on the desired geometry and material used for the final spun component required.
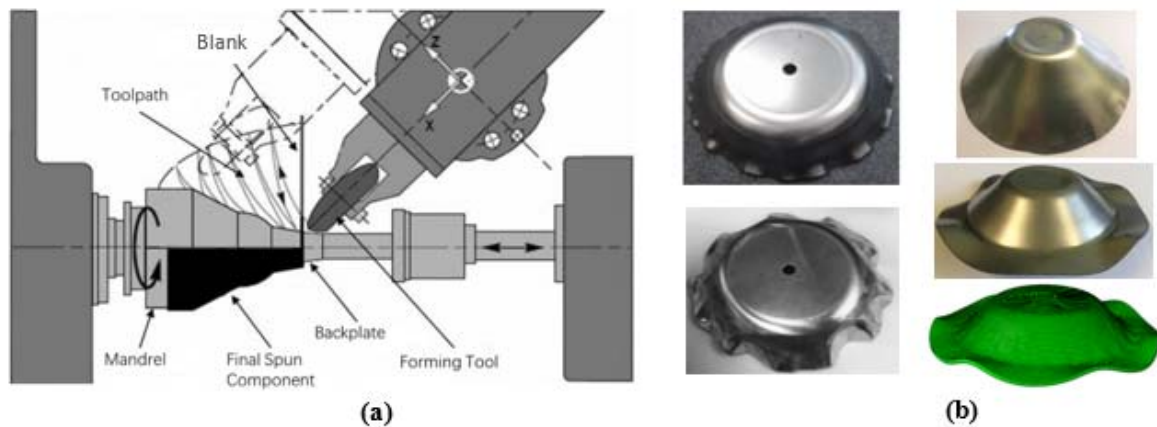
Fig. 1 Conventional sheet spinning: (a) typical process setup (Runge 1994); (b) wrinkled blanks by experiment and FE simulation (Wang and Long 2013, Childerhouse and Long 2019).

1.1 Wrinkling Studies in Spinning and Sheet Forming

Runge (1994) described wrinkling as one of the common process failures observed in the sheet metal spinning processes and Wong et al. (2003) reviewed these process failures in detail. A typical process setup of a multi-pass conventional spinning and examples of wrinkled spun parts are shown in Figure 1. To understand the mechanism of wrinkling in the conventional spinning process and effect of spinning process parameters on wrinkling, various studies have been undertaken using experimental, simplified analytical, and Finite Element (FE) simulation methods. Kobayashi (1963) stated that the material deformation modes in the conventional spinning process were similar to those of the deep drawing process. Kleiner et al. (2002) reported that the dynamic effect seemed to amplify the sensitivity of wrinkling during the spinning process. Sebastiani et al. (2006) observed the toothed pattern of the circumferential stresses in the FE simulation model, and stated that this stress pattern in the flange of the blank could be the pre-state of wrinkling. Xia et al. (2005) experimentally confirmed that wrinkling was more likely to occur in spinning processes when a high roller feed rate and a thin blank were used. Zhan et al. (2007) and Essa and Hartley (2010) conducted FE simulations and reported similar results. By performing both FE simulation and experiments, Wang et al. (2011) reached the same conclusion of the effect of the roller feed rate on wrinkling initiation. Several studies reported the significant effects of the feed ratio in spinning, defined as the roller feed rate per revolution of the mandrel. Hayama (1981) reported that the feed ratio, thickness and diameter of the blank were very important factors for wrinkling in the shear spinning process. Xia et al. (2005) produced experimental results investigating the effect of feed ratio on the forming forces in one-pass deep drawing spinning. Kong et al. (2017) performed experiments to verify the effect of feed ratio on flange wrinkling in first-pass conventional spinning of a hemispherical part and confirmed that the use of low feed ratios reduced the risk of wrinkling. Wang et al. (2011) reported the effect of feed ratio on wrinkling initiation and thickness variation of spun parts in a 3-pass conventional spinning and produced a feed ratio limit diagram based on FE simulation results. Childerhouse and Long (2019) showed the effect of feed ratio on surface finish and wrinkling of the blank in an experimental study. It concluded that applying higher feed ratios was the predominant factor in the cause of wrinkling of the blank and that the wrinkling severity increased with an increased feed ratio. High feed ratios also led to rougher surfaces of spun parts. There existed a feed ratio limit when spinning a specific geometry and a material, when exceeded, wrinkling occurred.

Blank wrinkling is a material processing failure commonly observed in other sheet metal forming processes and considered as one of the plastic instability problems. Tomita (1994) produced a comprehensive review of computational predictions related to the plastic instabilities, including wrinkling of thin plates and shells during sheet forming processes. Senior (1956) developed an analytical model to study wrinkling in a deep drawing process based on the method of energy conservation. In this model, the wrinkling waveform was established and the energy consumed under wrinkling conditions was determined. The critical condition of wrinkling was obtained when the internal energy of the blank, including bending deformation and circumferential shrink deformation, equated to the external energy produced by the lateral loading applied on the flange surface by forming tools. However the developed model was based on the one-dimensional buckling analysis thus the radial stresses of the blank were neglected. Hutchinson and Neale (1985) stated that wrinkling could be considered as a plastic buckling process and the material deformation mode depended on the local curvatures and thickness of the blank. By applying the Donnell-Mushtari-Vlasov theory for thin shells (Novozhilov, 1964), simple formulations for the stresses or strains at the onset of wrinkling were produced, based on the assumptions that the principal axes of the membrane stress state coincided with the principal axes of the doubly-curved metal sheet, free of any contact with tools. This work showed potentials of employing the Donnell-Mushtari-Vlasov theory for predicting wrinkling in sheet forming processes where the deforming sheet had a doubly-curved shell. Tugcu et al. (2001) expanded the work developed in Hutchinson and Neale (1985) by considering the sheet planar anisotropy using the anisotropic yield criterion Barlat-91. Parametric studies were performed to generate numerical results for critical stress states under various loading conditions and the results showed that the highly nonlinear nature of the predictions, especially when both principal stresses were compressive. Although the predictions were more sensitive to the orientation of the axes of anisotropy for stress states resulting in compressive stresses along both principal stress directions, the effect of the planar anisotropy on the onset of wrinkling was not clear. Wang and Cao (2000) developed an analytical approach for predicting the onset of flange wrinkling when a metal sheet was under normal constraints by using a combination of energy conservation and plastic bending theory. The analytical approach enabled the analysis of material deformation in the regions involving the contact between sheet and forming tool thus overcoming the limitation of the non-contact model developed by Hutchinson and Neale (1985). The analytical model developed by Wang and Cao (2000) produced the prediction of the critical buckling stress and wavelength as functions of normal pressure which was a critical consideration in determining the blank holding force and designing drawbeads in deep drawing process. To predict the onset of wrinkling during a shrink flanging operation, Wang et al. (2001) established a curved sheet model to obtain the critical buckling stress in terms of stress state, geometrical and material properties. The prediction of the critical flange length showed that it was significantly influenced by the plan view radius, sheet thickness and material work-hardening, but was not sensitive to material strength and anisotropy. The aforementioned analytical models provide the fundamental understanding of wrinkling mechanism and material deformation in sheet forming processes, however, they are not suitable for spinning due to their inability to consider various spinning toolpath profile designs commonly used in spinning and multi-passes required in the conventional spinning process.

1.2   Prediction of Onset of Wrinkling in Spinning

The forming limit diagram (FLD), defined by using the principal strains of the blank during forming, is widely used to identify safe and failure regions in various sheet forming processes. For example, Hosford and Duncan (1999) created the FLDs for the deep drawing process, Shim and Park (2001) presented FLD comparisons between sheet forming processes and incremental sheet forming process. Kegg (1961) proposed a test method to obtain the maximum strains without fracture thus to determine the spin ability of the material in shear spinning. However, Hayama and Tago (1968) reported the limitation of this spin ability test method because it was invalid for other mandrel geometries. Similarly, the processing map defining the relationship between formability and key process parameters is developed in the sheet metal forming processes. However, limited research is conducted to study processing maps in the conventional spinning process. Xia et al. (2005) proposed a processing map for avoiding both fracture and wrinkling failure by considering the effect of the material properties, feed ratio, and drawing ratio in the experiment of one-pass deep drawing spinning. Wang et al. (2011) obtained a processing map to prevent wrinkling failure by applying different combinations of the roller feed rate and mandrel rotational speed based on FE simulation results. Childerhouse and Long (2019) experimentally developed processing maps to produce wrinkle-free parts in shear spinning. Chen et al. (2019) presented an analytical model to determine the formability and to prevent wrinkling in first-pass conventional spinning, using linear toolpaths. Because of employing a simplified linear toolpath profile that was commonly used in shear spinning as well as defining the forming limit by using the half cone angle of the spun geometry, the results obtained were insufficient for practical applications because they focused only on specific spinning process conditions and spinning geometries. However, through these studies, the key spinning process parameters affecting wrinkling were identified and it showed that the processing maps were a useful tool to prevent wrinkling failure when operating under different spinning process conditions.

To study the material deformation and wrinkling prediction in spinning, the experimental test and the FE simulation methods have been commonly employed. For practical applications, both methods are time-consuming and resource-expensive when compared to an analytical method. Limited research has been reported to establish an analytical model for investigating wrinkling failure in spinning. This is due to the existence of non-uniformly distributed material stresses and strains in the blank and nonlinear load-deflection relationships under complex process conditions in spinning. Kong et al. (2017) proposed an analytical wrinkling prediction model based on the plastic buckling theory and the energy conservation for first-pass conventional spinning of a hemispherical part. A doubly-curved surface model, located at the tool-blank contact zone between the deformed and undeformed flange region of the blank, was established. However, the boundary conditions of this analytical model were extracted from FE simulation results, which required multiple time-consuming simulations thus impractical for applications. Chen et al. (2021) developed a theoretical prediction model based on the generalized variation principle of limit analysis to determine the critical circumferential stress which was then compared to the instant maximum circumferential stresses in the zone affected by the roller action to predict the flange wrinkling in the conventional spinning. However, a FE simulation model was required for the calculation of both the critical circumferential stress and the maximum circumferential stresses in the flange. Based on the analysis of stresses and strains, Chen et al. (2019) proposed an analytical model to predict wrinkling in the first-pass conventional spinning using linear toolpaths. The critical condition of wrinkling was determined by comparing the maximum circumferential stress and the

critical circumferential stress of the blank in spinning. Compared to the analytical models established by Kong et al. (2017), the models developed by Chen et al. (2019) and Chen et al. (2021) considered the stresses located at the flange of the undeformed region of the blank, instead of being located at the tool-blank contact zone. Compared to Kong et al. (2017) and Chen et al. (2021), Chen et al. (2019) obtained the relationship between the wrinkling and the spinning process parameters directly without the need of relying on developing and running time-consuming FE simulation models which could be forbidden in practical applications. Therefore, an analytical prediction method without the need of using FE simulations is more effective in the prediction of wrinkling in spinning applications.

By reviewing studies on material deformation mechanics in spinning, Music et al. (2010) reported that to avoid wrinkling, it was desirable to achieve a balanced combination of radial tensile stresses and circumferential compressive stresses of the blank during the conventional spinning process. Wang and Long (2013) produced FE simulation results of stress and strain distributions to evaluate the material deformation modes during spinning. Kong et al. (2017) developed FE simulation and theoretical prediction to study circumferential compressive stresses distributed in the flange of spun parts. In general, the balanced material deformation can be achieved by employing multiple tool passes in the conventional spinning process. However, the determination of the exact number of tool passes required for a specific spun geometry of a specific material still involves many trial and error experimental tests and often relies on empirical knowledge of spinners developed over many years of practice. In addition, the design of roller toolpath profiles is a crucial decision in the conventional spinning process because they have a significant effect on the spun part quality and process failures, including both wrinkling and fracture. Hayama et al. (1970) experimentally investigated the effect of four different toolpath types, linear-revolved, circular-outside shifted, circular-inside shifted, and linear-inside shifted. It was concluded that the use of an involute toolpath, a type of a convex curve, allowed large diameters of the blank to be spun without wrinkling failure. Kawai and Hayama (1987) experimentally studied spinning roller passes for producing cylindrical hollow parts and concluded that an involute toolpath was capable of creating a sound final part free of wrinkles in the flange and fractures in the wall of the spun part. Consistent results by employing convex toolpath designs to avoid wrinkling and to improve quality of spun parts were also reported in a number of other studies. For example, Liu et al. (2002) produced FE simulation of stress distributions using three different path designs, Wang and Long (2013) investigated the effects of toolpath profiles on thickness, spinning forces and wrinkling, Polyblank and Allwood (2015) developed parameterised toolpaths and evaluated their effects on thickness, tool force and wrinkling. A number of studies reported that the wrinkling prevention during first pass of a multi-pass conventional spinning is essential to ensure a successful spinning. These included that Kawai and Hayama (1987) developed roller passes by NC programming, Watson et al. (2015) found the involute roller path of an angle of 40° to be the optimum for the first pass by applying the BoxBehnken design of experiments in FE simulation. Toolpath design in many existing studies relied on the empirical design of toolpath profiles to achieve individual spun part geometries. In three recent studies, Li et al. (2014) firstly adopted the quadratic Bézier curve to parameterise the toolpath profile design for the first-pass of the multi-pass spinning. Polyblank and Allwood (2015) also used the Bézier curve based toolpath profile parameterisation for the first pass, while Gan et al. (2016) worked on the two-pass conventional spinning. However, these studies mainly focused on investigating the effect of the toolpath profiles on

the roller tool forces, the accuracy of the spun part geometry and thickness distribution but not aimed at developing an effective wrinkling prediction method for the multi-pass conventional spinning.

This paper develops an analytical wrinkling prediction model integrated with toolpath design to support the process design and parameter selection in the development of multi-pass conventional spinning. The toolpath profile design is parameterised based on the cubic Bézier curve that is capable of producing concave, convex, and linear toolpath profiles with a varied path curvature. It is proposed that the forming depth of the designed toolpath profile in each pass is a critical variable to avoid wrinkling. A wrinkling-wave function is developed to capture the geometrical characteristics of a wrinkled blank and to enable the analysis of material plastic deformation during first-pass conventional spinning using a concave toolpath profile. The critical condition of the onset of the wrinkling, defined as the critical forming depth, is determined based on the instability condition of the blank by equating the strain energy of the blank deformation and the energy produced by the forming force of the spinning tool. By employing the wrinkling prediction model, effects of material properties and blank geometrical parameters, feed ratio, and spin ratio in the first-pass of the conventional spinning using a concave toolpath profile are investigated. It has been found that the critical forming depth is affected by the spin ratio significantly, followed by the blank thickness and the feed ratio. The developed analytical wrinkling prediction model is further experimentally validated using different toolpath profiles, including concave, convex, and linear toolpaths, under various spinning process conditions by developing test runs using the technique of the Design of Experiments. Three-dimensional processing maps to prevent wrinkling are produced for the first-pass conventional spinning using a concave toolpath profile. The results demonstrate the potential of the developed wrinkling prediction model integrated with toolpath design to support the spinning process development for practical applications.

2. Critical Forming Depth in Designing Toolpath Profile

The toolpath profile design in sheet spinning processes is an essential step in manufacturing spun parts of various geometries. The most frequently used toolpath profiles can be categorised as concave, convex, and linear toolpath profiles. In this study, the multi-passes of the conventional spinning process are realised by independently defining individual toolpath profiles and forming depths to deform the blank that create the desired spun geometry. The cubic Bézier curve is adopted to generate concave, convex, and linear toolpath profiles. Four control points are required to produce a cubic Bézier curve thus to uniquely define a toolpath profile, as shown in Figure 2a. The path curvature of the cubic Bézier curve is defined as $PC = \pm\lambda, \pm2\lambda \cdots$, where a positive and negative sign produces a concave and convex profile respectively; and for a linear profile, PC = 0. By applying a specific value, λ, as the path curvature, the individual toolpath profile, whether a concave, convex or linear curve, can be produced. Figure 2b shows a concave toolpath profile with a path curvature of $+2\lambda$ for an arbitrary tool pass i. Figure 2b also shows the definition of the forming depth, h_i, and this study proposes that its value is critical in the prediction of the onset of wrinkling for a toolpath profile designed.

As shown in Figure 3, the contour lines produced by the tool when in contact with the blank surface using concave, linear and convex toolpath profiles are created to illustrate the effect of the feed ratio on the interaction between the tool and the blank. A higher feed ratio creates an increased step of the roller in contact with the blank surface that results in a greater distance on the blank surface in the axial

direction (OO') per mandrel revaluation thus more pronounced tool contact marks. Chen et al. (2019) reported the same observation by developing the analytical prediction and Childerhouse and Long (2019) experimentally confirmed this finding. A greater distance between the tool contour lines using a high feed ratio leads to a greater circumferential force of the roller tool required to deform the blank material in each mandrel rotation thus a greater increment of the external energy produced by the roller tool in progressing to the unstable condition of the blank, consequently a higher risk of wrinkling.
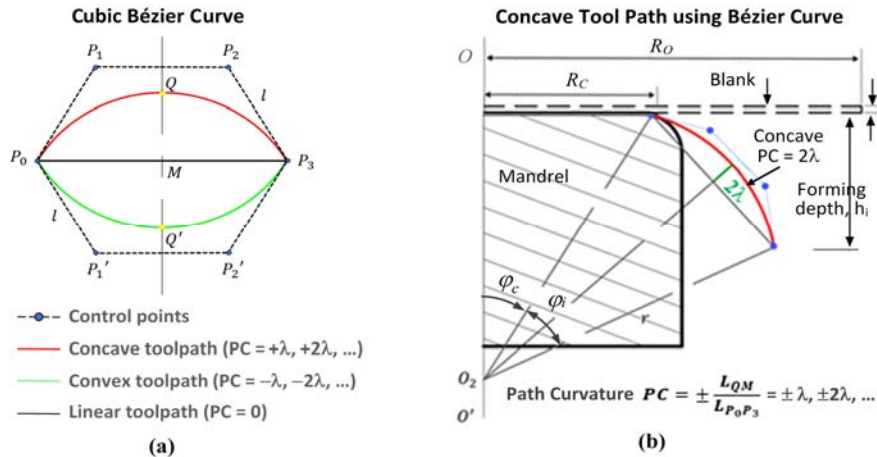
Fig. 2 Generation of toolpath profiles (a) cubic Bézier curve for various toolpaths; (b) concave toolpath (where R_O and t are radius and thickness of original blank; R_C is radius of the blank clamping area and φ_C is the angle defining clamping end point; h_i is forming depth; φ_i is subtending angle of the concave toolpath).
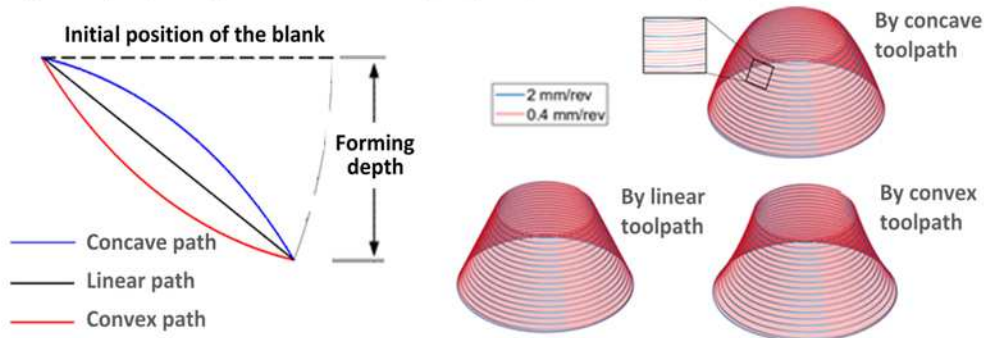
Fig.3 Spun surfaces created by tool contact contour lines using concave, linear and convex toolpath (where the feed ratio is arbitrarily selected as $2\ mm/rev$ and $0.4\ mm/rev$ respectively)

The proposed toolpath profile generation method can be used for any pass of a multi-pass conventional spinning, including the first-pass and the final-pass. In the following sections in developing the analytical wrinkling prediction model, only the first-pass is presented because the previous studies have confirmed that the prevention of wrinkling failure during the first pass of a multi-pass conventional spinning is critical for the process to be successful. The toolpath profile selected is a concave toolpath because consistent results have shown that employing convex toolpath designs can better prevent the wrinkling, as discussed in the Introduction. Therefore, a concave toolpath could be considered as the worst case in designing toolpaths. If the wrinkling could be avoided by employing a concave toolpath under a specific forming depth in the first-pass of a multi-pass spinning process, then applying a convex or linear toolpath with the same forming depth, as illustrated in Figure 3, should also avoid the wrinkling. This assumption will be tested in Section 5.2 by performing both the wrinkling prediction and analysis as well as the first-pass conventional spinning experiment when the concave, linear and convex toolpaths are employed.

3. Definition of Wrinkling Wave Function

Both experimental and FE simulation of wrinkled parts in the sheet spinning processes are produced as shown in Figure 1b. It shows that a wrinkled part has waveforms varying periodically in the circumferential direction. A spun part can be defined by its middle surface as shown in Figure 4a, based on the thin shell theory by Timoshenko and Woinowsky-Krieger (1959). For a wrinkle-free spun part, the middle surface is defined as a doubly-curved shell structure with thickness t, created by a concave toolpath, as shown in Figure 4b. Any point on the middle surface can be defined by local coordinates x and y, coincided with the directions of principal curvatures of the shell structure in the circumferential direction and the meridional direction, respectively, while coordinate z is normal to the middle surface. The displacements in the x, y and z directions are defined as u, v, w respectively.

To capture the geometrical features of a wrinkled blank as observed from the spinning experiment and FE modelling as shown in Figure 1b, wrinkle-waves of a spun part may be described by a doubly curved surface using a cosine function along the circumferential direction and a sine function along the meridional direction of the middle surface, as shown in Figure 4c. The wrinkle waves are assumed to be uniformly distributed thus the number of wrinkle-ridges and wrinkle-bottoms along the circumferential direction can be defined as m.

To define wrinkle-waves quantitatively, amplitudes of a wrinkle-ridge and a wrinkle-bottom along the circumferential direction are defined as $\Delta h_{\theta,r}$ and $\Delta h_{\theta,b}$ respectively, as shown in Figure 5b. These amplitudes refer to the distance between edges of the wrinkle-free and wrinkled cross-section surfaces. The clearance between the wrinkle-free and wrinkled cross-section surfaces along the meridional direction r_1 is defined as Δh_{φ}, as shown in Figure 5d. Theoretically, the value of $\Delta h_{\theta,r}$ should be zero thus the wrinkle-wave amplitude s is defined by the distance between the outer edge of the wrinkle-ridge and the wrinkle-bottom cross-section surfaces, as shown in Figures 5b and 5d.
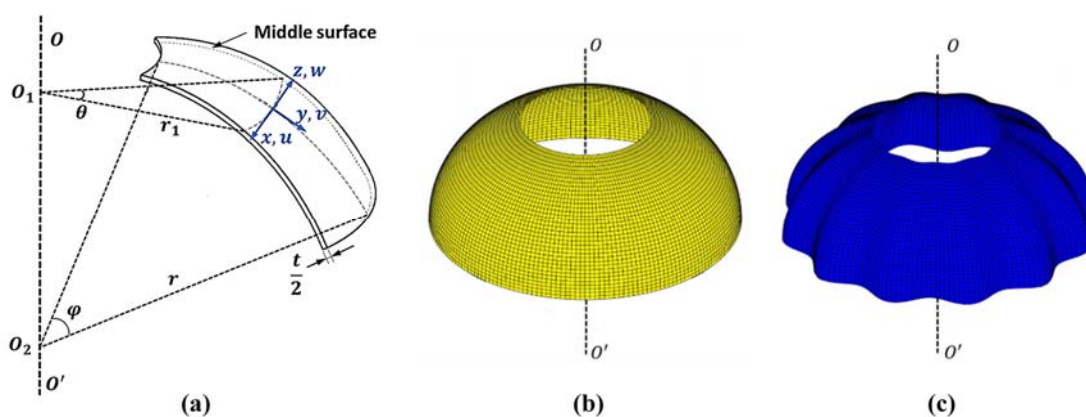
Fig. 4 Definition of spun geometry: (a) middle surface; (b) wrinkle-free surface; (c) wrinkled surface (r_1 and r are the principal radii along the circumferential direction and the meridional direction, respectively; θ and φ are the circumferential angle and the meridional angle, respectively).
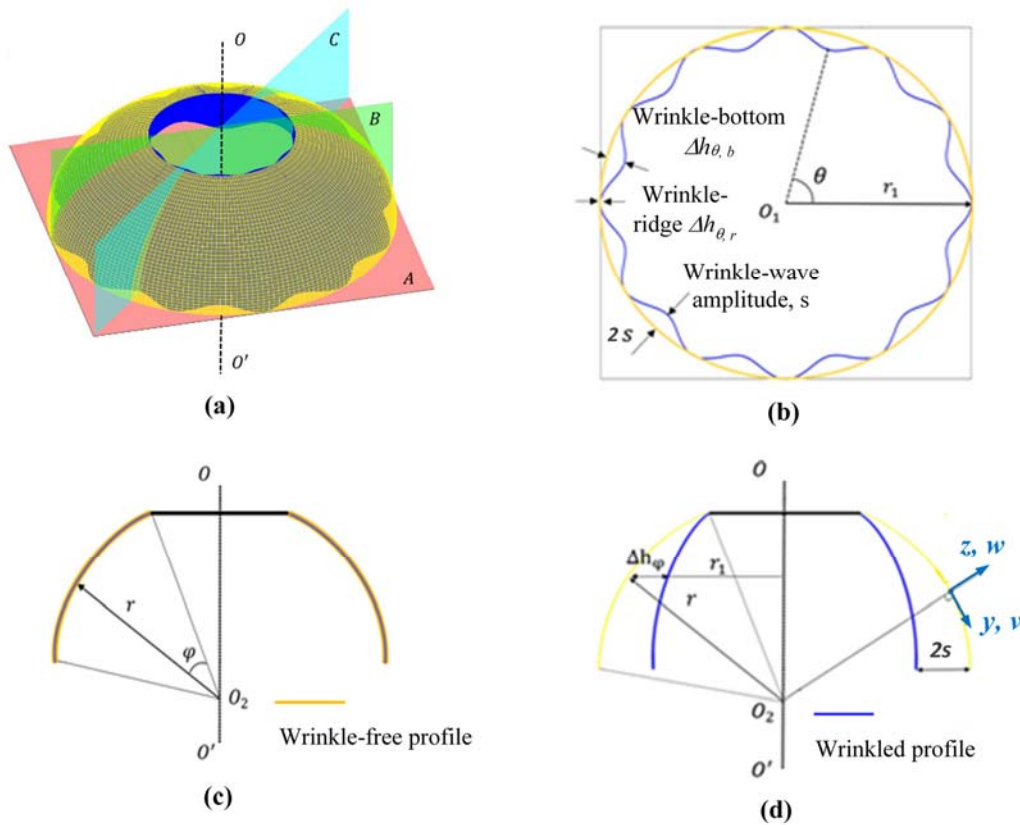
Fig. 5 Definition of wrinkle variables: (a) wrinkle-free and wrinkled surfaces; (b) A-A cross-section view; (c) B-B cross-section view; (d) C-C cross-section view ($\Delta h_{\theta,r}$ and $\Delta h_{\theta,b}$ are wrinkle-ridge and wrinkle-bottom amplitudes; s is wrinkle-wave amplitude; Δh_{φ} is clearance between wrinkle-free and wrinkled surfaces).

To define the wrinkle-wave function, the displacement normal to the middle surface of the spun part in the z direction, w, is adopted. The normal displacement $w(r, \theta, \varphi)$ must satisfy certain boundary conditions: it equals to zero at the edge of the clamped area of the blank and on the wrinkle-ridges:

$$\text{when} \ \ w = 0, \ \frac{\partial w}{\partial \varphi} = 0, at \ \varphi = 0 \quad \text{and} \quad \frac{\partial w}{\partial \theta} = 0, at \ \theta = \sum_{j=0}^{m} j \frac{2\pi}{m} \qquad (\text{Eq. 1})$$

Based on these boundary conditions, the wave function of a wrinkled spun part may be defined by

$$w = s \left[cos(m\theta) - 1\right] sin\left(\frac{\pi\varphi}{2\varphi_i}\right) \quad \text{and} \quad w_{\varphi=\varphi_i} = s \left[cos(m\theta) - 1\right] \qquad (\text{Eq. 2})$$

As shown in Figures 4a and 5d, s is the wrinkle-wave amplitude; m is the number of wrinkles; θ is the azimuthal angle in the circumferential direction; and φ is the zenith angle in the meridional direction and φ_i is the angle for the tool pass number i in a multi-pass conventional spinning process. By defining the wrinkle-wave function, the principal strains ε_θ and ε_φ, shear strain $\gamma_{\theta\varphi}$, the curvature changes κ_θ and κ_φ, and the twist χ of the deformed middle surface can be derived by adopting the Donnell-Mushtari-Vlazov theory (Novozhilov, 1964), a simplified deformation theory for thin shells. The expressions of these strain components of the middle surface are given in Appendix A.

The wrinkle-wave amplitude, s, at the outer edge of the wrinkled spun part is independent of φ and θ. By substituting $\varphi = \varphi_i$, the wave function represents the wrinkle-waves along the circumferential

direction at the outer edge of the blank can be simplified, as shown in Equation 2. By determining the perimeter of the outer edge of the wrinkled spun part and the perimeter of the outer edge of the wrinkle-free spun part, the total length of wrinkle-waves at the outer edge of a wrinkled spun part along the circumferential direction, Δl_{φ_i}, after the first-pass spinning can be determined:

$$\Delta l_{\varphi_i} = \int_0^{2\pi} R_2 \sqrt{1 + \left(\frac{1}{R_2}\frac{\partial w_{\varphi=\varphi_i}}{\partial \theta}\right)^2} \, d\theta - \int_0^{2\pi} R_2 \, d\theta \approx \frac{1}{2R_2}\int_0^{2\pi} \left(\frac{\partial w_{\varphi=\varphi_i}}{\partial \theta}\right)^2 d\theta = \frac{\pi s^2 m^2}{2R_2} \qquad \textbf{(Eq. 3)}$$

where R_2 is the radius of blank after first-pass of spinning and it can be expressed as $R_2 = r\sin(\varphi_C + \varphi_i)$, as illustrated in Figure 6a. **Considering $\Delta l_{\varphi_i} = 2\pi R_0 - 2\pi R_2$**, the amplitude of the wrinkle waves can be expressed as

$$s = \frac{2\sqrt{R_2(R_0 - R_2)}}{m} \qquad \textbf{(Eq. 4)}$$

By defining the forming depth in a parameterised toolpath profile and developing the wrinkling wave function, the geometrical parameters of a wrinkle-free and wrinkled blank can be determined. These will be used to analyse stresses and strains to determine the critical condition of the blank wrinkling.

4. Critical Condition of Wrinkling

Based on the elementary plasticity theory, the geometry of the blank deformation, the circumferential and the meridional stresses and strains are analysed. These are used to derive the critical forming depth of a concave toolpath at the onset of the wrinkling for the first-pass conventional spinning.

4.1 Analysis of Stresses and Strains

To predict wrinkling failure during first-pass conventional spinning process, stresses along the circumferential direction σ_θ and the meridional direction σ_φ in the plane of the deformed blank can be approximately assumed to be principal stresses (Hutchinson and Neale, 1985). The contact pressure induced by the roller on the blank in the thickness direction is assumed to be a small fraction of the material flow stress (Marciniak et al. 2002) thus insignificant in comparison with the tensile meridional stress and the compressive circumferential stress (Runge, 1994). Thus the principal stress in the blank thickness direction σ_t is determined by taking the average of the meridional stress and the circumferential stress. Second assumption made is that the strain in the thickness direction during conventional spinning can be considered small thus the thickness of the blank can be assumed to remain unchanged after deformation thus zero thickness strain. Finally friction between tool and blank contact surfaces is assumed negligible. Based on these assumptions, the principal strains and principal stresses of the deformed blank can be simplified as follows:

$$\begin{cases} \varepsilon_1 = \varepsilon_\varphi & \varepsilon_2 = \varepsilon_t = 0 & \varepsilon_3 = \varepsilon_\theta \\ \sigma_1 = \sigma_\varphi & \sigma_2 = \sigma_t = \dfrac{\sigma_\varphi + \sigma_\theta}{2} & \sigma_3 = \sigma_\theta \end{cases} \qquad \textbf{(Eq. 5)}$$

The principal strains of the middle surface of the deformed blank, the circumferential strain ε_θ and the meridional strain ε_φ, can be expressed by the wrinkling wave function $w(r, \theta, \varphi)$, developed in Section 3. Figure 6a illustrates the deformed geometry of the blank after the first-pass conventional spinning using a concave toolpath. The original radius of the blank is reduced from R_O to R_2. As a result, the

circumferential length is reduced and the flat sheet blank is formed by the concave toolpath into a doubly-curved surface with a forming depth. When the forming depth reaches a critical value, h_c, shown in Figure 6a, wrinkling occurs. Based on the geometrical relations of the blank before and after deformation, considering the volume consistency and the assumption of the blank thickness remains unchanged after the deformation, for an infinitesimal element of the deformed blank as shown in Figures 6a and 6b, the circumferential strain ε_θ and the meridional strain ε_φ can be derived as:

$$\varepsilon_\theta = ln\left(\frac{r_1}{\sqrt{R_C{}^2 + (R_C + r_1)\,r\varphi}}\right) \quad \text{and} \quad \varepsilon_\varphi = ln\left(\frac{\sqrt{R_C{}^2 + (R_C + r_1)\,r\varphi}}{r_1}\right) \tag{Eq. 6}$$

The equivalent strain resulted from the reduction of the circumferential length of the blank after the deformation can be written as:

$$\bar{\varepsilon} = -\frac{2}{\sqrt{3}}\varepsilon_\theta = \frac{2}{\sqrt{3}}\varepsilon_\varphi = \frac{2}{\sqrt{3}}\,ln\left(\frac{\sqrt{R_C{}^2 + (R_C + r_1)\,r\varphi}}{r_1}\right) \tag{Eq. 7}$$

Referring to the principal stresses as illustrated in Figure 6b, consider the force equilibrium of the infinitesimal element in the meridional direction, it leads to

$$r_1\,d\sigma_\varphi + (\sigma_\varphi - \sigma_\theta)\,dr_1 = 0 \tag{Eq. 8}$$

From the principal stresses expressed in Equation 5, the equivalent stress can be written as

$$\bar{\sigma} = \frac{\sqrt{3}}{2}(\sigma_\varphi - \sigma_\theta) \tag{Eq. 9}$$

The meridional stress σ_φ and the compressive circumferential stress σ_θ can be expressed as

$$\sigma_\varphi = \frac{2}{\sqrt{3}}\bar{\sigma}\,ln\frac{R_2}{r_1} \quad \text{and} \quad \sigma_\theta = \frac{2}{\sqrt{3}}\bar{\sigma}\left(1 - ln\frac{R_2}{r_1}\right) \tag{Eq. 10}$$

Considering the feed ratio must be controlled and kept below a certain limit to avoid the onset of wrinkling as discussed in Section 1.1, the effect of the rate-dependency of the blank material on wrinkling initiation is not considered in this study. By employing the material constitutive equation $\bar{\sigma} = K\bar{\varepsilon}^n$, the compressive circumferential stress σ_θ can be expressed as

$$\sigma_\theta = K\left(\frac{2}{\sqrt{3}}\right)^{n+1}\left(ln\left(\frac{\sqrt{R_C{}^2 + (R_C + r_1)\,r\varphi}}{r_1}\right)\right)^n\left(1 - ln\frac{R_2}{r_1}\right) \tag{Eq. 11}$$

where K is the strength coefficient and n is the strain-hardening coefficient of the blank material respectively. The geometrical parameters of R_O, R_C, R, R_2, φ_C, φ, φ_i, r and r_1 are defined as shown in Figure 6a.
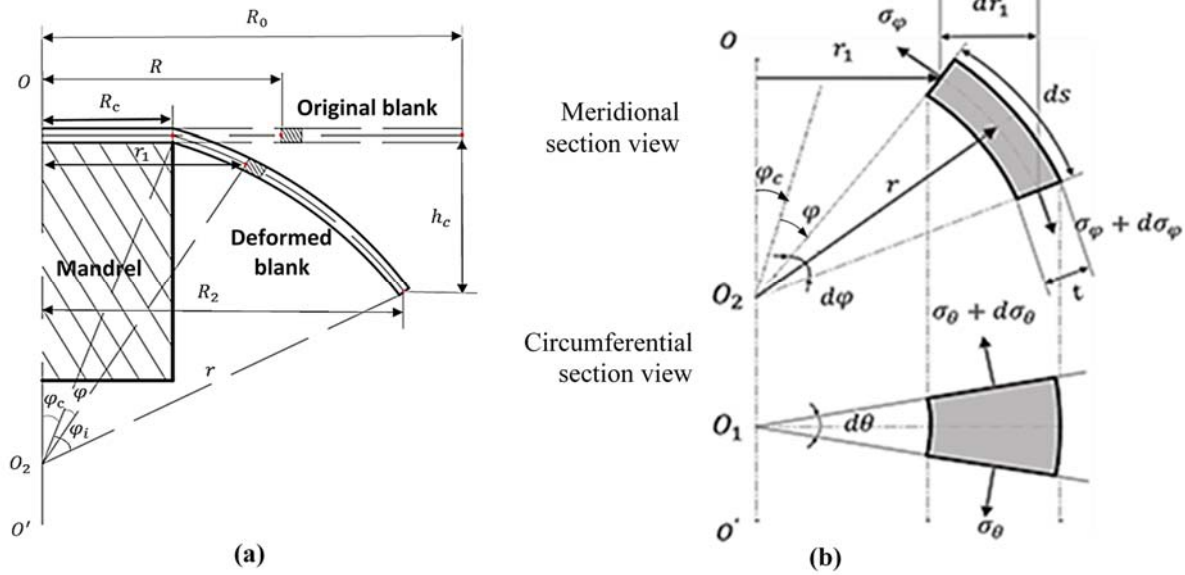
Fig. 6 Analysis of blank deformation and stresses acting on an infinitesimal element
(where R_0 is the original radius of blank; R_2 is the radius of blank after first-pass of spinning, $R_2 = r\sin(\varphi_C + \varphi_i)$; R_C is the radius of clamped area; h_c is the critical forming depth of first-pass spinning; for the infinitesimal element, $ds = r\,d\varphi$; $r_1 = r\sin(\varphi + \varphi_c)$, $dr_1 = r\,d\varphi\,\cos(\varphi + \varphi_c)$).

4.2   Wrinkling Criterion

By applying the expression of the strain energy for a doubly-curved thin shell (Novozhilov, 1964), the strain energy required for the blank to wrinkle, U, can be derived as shown in Appendix B. By replacing stress and strain variables as shown in Equations 5, 6, 10, 11 and the wrinkling wave function as shown in Equation 2, a simplified expression of the strain energy can be shown as

$$U = s^2\left(A_1 m^4 + A_2 m^2 + A_3\right) = 4\,R_2(R_0 - R_2)\left(A_1 m^2 + A_2 + \frac{A_3}{m^2}\right) \qquad \text{(Eq. 12)}$$

where m is the number of wrinkles (Equation 1); s is the wrinkle-wave amplitude (Equation 4); A_1, A_2, A_3 are parameters and their expressions are given in Appendix B. These parameters can be determined by the material properties, the geometrical parameters of the original blank and wrinkled blank after the first-pass spinning. From Equation 12, by performing differentiation of U over m and letting $\partial U/\partial m = 0$, the critical number of wrinkling waves of the blank, m_c, can be obtained as

$$m_c = \sqrt[4]{\frac{A_3}{A_1}} \qquad \text{(Eq. 13)}$$

Therefore the minimum strain energy required for the blank to wrinkle, U_{min}, can be determined by

$$U_{min} = 4R_2(R_0 - R_2)\left(A_1 m_c{}^2 + A_2 + \frac{A_3}{m_c{}^2}\right) \qquad \text{(Eq. 14)}$$

The external work done by the spinning tool when forming a wrinkle-free blank can be determined

$$T = \int \Delta F_\theta\,\Delta L_\theta \quad \text{and} \quad \Delta F_\theta = |\sigma_\theta|\,r\,t\,d\varphi \qquad \text{(Eq. 15)}$$

where ΔF_θ is the circumferential compressive force acted on the infinitesimal element of the blank, ΔL_θ is the circumferential length reduced from the original blank to the deformed blank. Based on the geometrical relations before and after the deformation, it can be shown

$$\Delta L_\theta = 2\pi \left(\sqrt{R_C{}^2 + (R_C + r_1)\, r\varphi} - r_1 \right) \tag{Eq. 16}$$

Taking the feed ratio f into account, the total number of rotations of the blank for completing the first-pass conventional spinning can be expressed as $N_i = r\,\varphi_i/f$ and the required number of rotations to deform the blank to the specific location of an infinitesimal element can be written as $N_{ik} = r\varphi/f$, $N_{ik} \le N_i$. The work done by the spinning tool in deforming the blank can be derived as

$$T = 2\pi t f \int_0^{N_i} K\left(\frac{2}{\sqrt{3}}\right)^{n+1} \left| \left(\ln \frac{\sqrt{R_c{}^2 + (R_C + r_{1,ik})N_{ik}\, f}}{r_{1,ik}} \right)^n \left(1 - \ln \frac{r_{1,i}}{r_{1,ik}} \right) \right| \left(\sqrt{R_c{}^2 + (R_C + r_{1,ik})N_{ik}\, f} - r_{1,ik} \right) dN_{ik}$$

$$\tag{Eq. 17}$$

where $r_{1,i} = r\,\sin(N_i f / r + \varphi_C)$ and $r_{1,ik} = r\,\sin(N_{ik} f / r + \varphi_C)$ are the principal radius along the circumferential direction to complete the first-pass of the spinning and to deform the blank to the specific location of an infinitesimal element, respectively.

Based on the stability theory by Timoshenko and Gere (1961), if the work done by the spinning tool in deforming the blank, T, is less than the minimum strain energy required for the blank to wrinkle, U_{min}, the equilibrium of the doubly-curved surface represented by the wrinkling wave function is stable, which leads to a wrinkle-free spun part. Otherwise, the condition becomes unstable and wrinkling will occur in deforming the blank. Therefore, the critical condition to generate a wrinkle-free spun part can be obtained when $T \le U_{min}$. By solving this equation, the critical forming depth, h_c, can be obtained as

$$h_c = \sqrt{\left(2r \sin \frac{\varphi_i}{2}\right)^2 - (r \sin(\varphi_C + \varphi_i) - R_C)^2} \tag{Eq. 18}$$

The calculation of the critical forming depth for the first-pass of a conventional spinning using a concave toolpath can be performed by firstly selecting an initial value of the meridional radius $r = (r_{lower} + r_{upper})/2$ where r_{lower} and r_{upper} are the upper and lower limit of r, which depend on the radius of the original blank. The second step is to calculate the strain energy required for the blank to wrinkle, U, and the work done by the spinning tool in deforming the blank, T. If $U - T \ne 0$ and $U - T < 0$, then replace r with r_{upper} to repeat the calculation of U and T using the updated r. If $U - T \ne 0$ and $U - T > 0$, then replace r with r_{lower} to repeat the calculation of U and T using the updated r. When $U - T = 0$ is satisfied, determine the geometrical parameters of the blank (r, φ_C, φ_i) to calculate the critical forming depth h_c. In this study, the key equations are written in MATLAB codes to perform the above calculations.

4.3 Experimental Validation of Wrinkling Prediction Model

To validate the developed analytical wrinkling prediction model integrated with toolpath design, an experiment of the first-pass conventional spinning is conducted on a CNC turning centre, as shown in Figure 7. To detect the initiation of wrinkling during the spinning process, a vibration sensor (PCB Piezotronics) is attached to the tool holder to monitor and record vibration signals generated by the blank on the roller tool. A sensor signal conditioner and oscilloscope are employed to convert vibration signals into a digital waveform and its changes are used to detect the wrinkling initiation. The experimental validation considers the key spinning process parameters and their variations including the path curvature of convex, linear and concave toolpath, blank thickness, feed ratio, spin ratio, as

shown in Figure 7. To reduce the number of experimental test runs in a full factorial experiment, a D-optimal Design of Experiments is employed to generate experimental test runs to consider the combination of variation levels of these process parameters and this is detailed in Table 1.
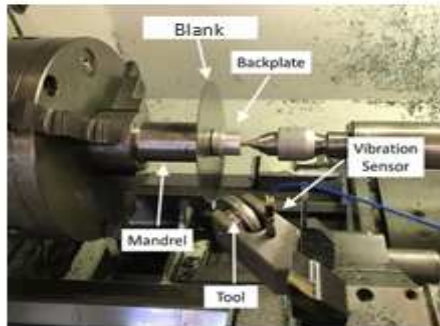
Level	Thickness (mm)	Feed Ratio (mm/rev)	Path Curvature	Spin Ratio
Low	1.2	0.5	-2λ	0.73
Intermediate	1.5	1	0	-
High	2	1.5	$+2\lambda$	0.80
No. of test runs of the full factorial experiments = 3^3 = 27				No. of extra
No. of test runs of D-optimal Design of Experiments = 13				runs = 5

Fig. 7 Experimental setup on CNC turning machine and variation of key spinning variables

5. Results and Discussion

In this section, wrinkling results obtained from the analytical prediction model using a concave toolpath profile and experimental tests using convex, linear and concave toolpath profiles in the first-pass conventional spinning are presented and discussed.

5.1 Preliminary Results of Wrinkling Prediction Model

The wrinkling prediction model is firstly tested to evaluate the effect of blank material on the onset of wrinkling. The blank material of mild steel (DC01) and aluminium alloys (AA5052 and AA1050) are used. The strain energy of the blank deformation and the external energy of the work done by the spinning tool in the first-pass conventional spinning using a concave toolpath profile are calculated as shown in Figure 8. The critical forming depth is obtained when the line of the external energy produced by the spinning tool intersects with the line of the strain energy of the blank. Under the same spinning process conditions, DC01 is capable of reaching a higher critical forming depth than both AA5052 and AA1050 at the onset of wrinkling while AA1050 has the lowest critical forming depth. DC01 has a higher strain-hardening coefficient than that of AA5052 and AA1050 which implies that the strain hardening has a greater effect on the wrinkling resistance than other material properties. The reason for this is that the strain hardening effect increases the yield strength of the blank material under greater plastic strains, the circumferential stresses within the blank also increase, which leads to a higher minimum strain energy for the blank to wrinkle (i.e. a higher U_{min}). Therefore, a material with a higher strain-hardening coefficient is more resistant to wrinkling failure.
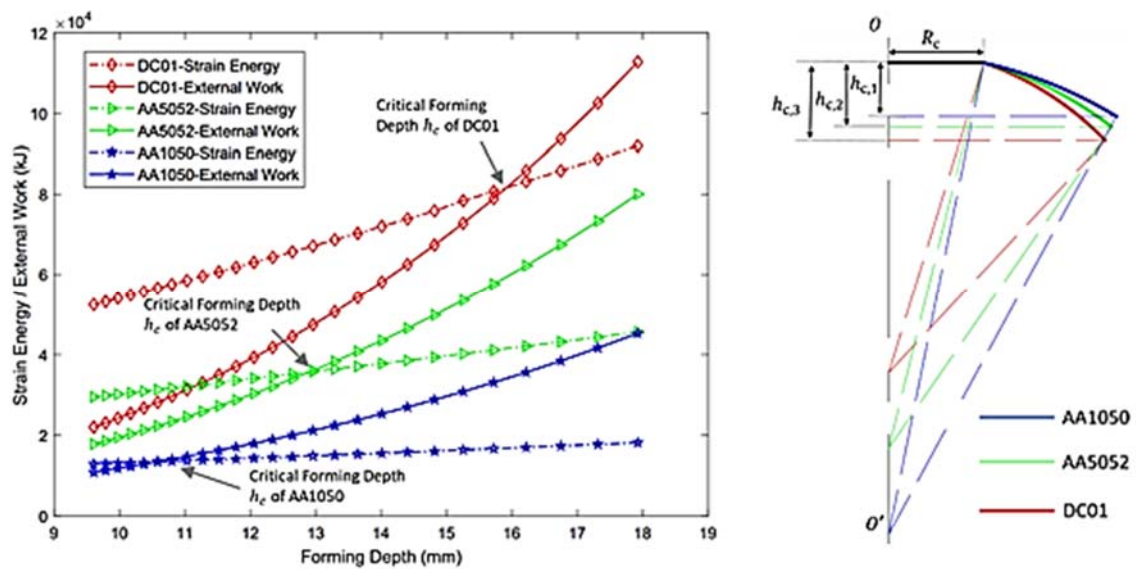
Fig. 8 Effect of blank material on the critical forming depth of first-pass using concave toolpath (where $h_{c,1}, h_{c,2}$ and $h_{c,3}$ are the critical forming depth of AA1050, AA5052 and DC01; R_O =50 mm, R_C =20 mm, t = 1.2 mm are the blank original radius, clamping radius and thickness, respectively).

Secondly, the wrinkling prediction model is tested to evaluate the effect of spinning process parameters on the onset of the wrinkling. This includes investigating effects of the original blank radius and thickness as well as the feed ratio on the critical forming depth. Under an increasing radius of the original blank, the critical forming depth shows a clear increasing trend for all materials, as shown in Figure 9a. As the wrinkling occurs only by the formation of wrinkles in the un-spun flange of the blank, to evaluate the effect of the unsupported flange dimension, two new variables are defined. The spin ratio, $\tau = (R_O - R_C)/R_O$, is introduced by considering the original blank radius R_O and the radius of the clamped area of the blank R_C. The wrinkling sensitivity ratio, $\eta = (R_O - R_C)/h_c$, is introduced to analyse the effect of the spin ratio on wrinkling; the higher the wrinkling sensitivity ratio is, greater sensitivity of a blank to wrinkling. The same data in Figure 9a is redrawn by using the wrinkling sensitivity ratio and the spin ratio, as shown in Figure 9b. With the increase of the spin ratio, the wrinkling sensitivity ratio increases significantly. Therefore, it is clear that the wrinkling is sensitive to the dimension of the unsupported flange of the blank. If the thickness remains the same, a blank with a larger radius using the same clamping radius is more likely to wrinkle during spinning.

Figure 10a shows the effect of blank thickness on wrinkling. A thicker blank has an increased rigidity thus leads to a significant increase of the critical forming depth. Figure 10b shows that the critical forming depth decreases with the increase of the feed ratio. This is because the larger the feed ratio is, the greater compressive circumferential stresses are; which requires the greater external work done by the spinning tool in deforming the blank. This agrees with the conclusion of the previous studies that using higher feed ratios increases the risk of wrinkling, Kong et al. (2017), Wang et al. (2011), and Childerhouse and Long (2019).
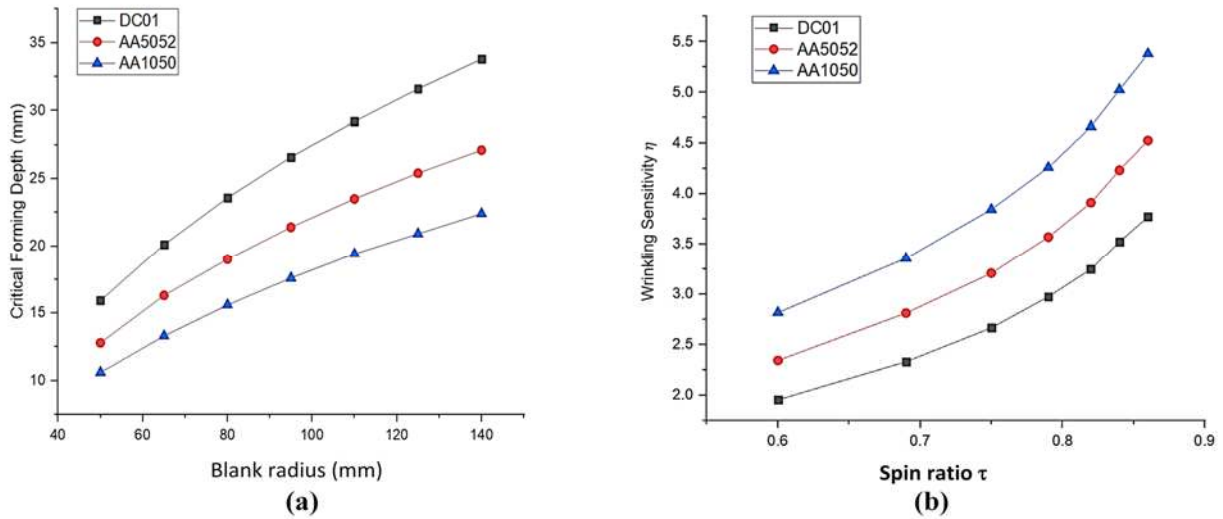
Fig. 9 Effect of blank radius / spin ratio on wrinkling (R_C =20 mm, t = 1.2 mm)
(a) critical forming depth vs. blank radius; (b) wrinkling sensitivity vs. spin ratio.
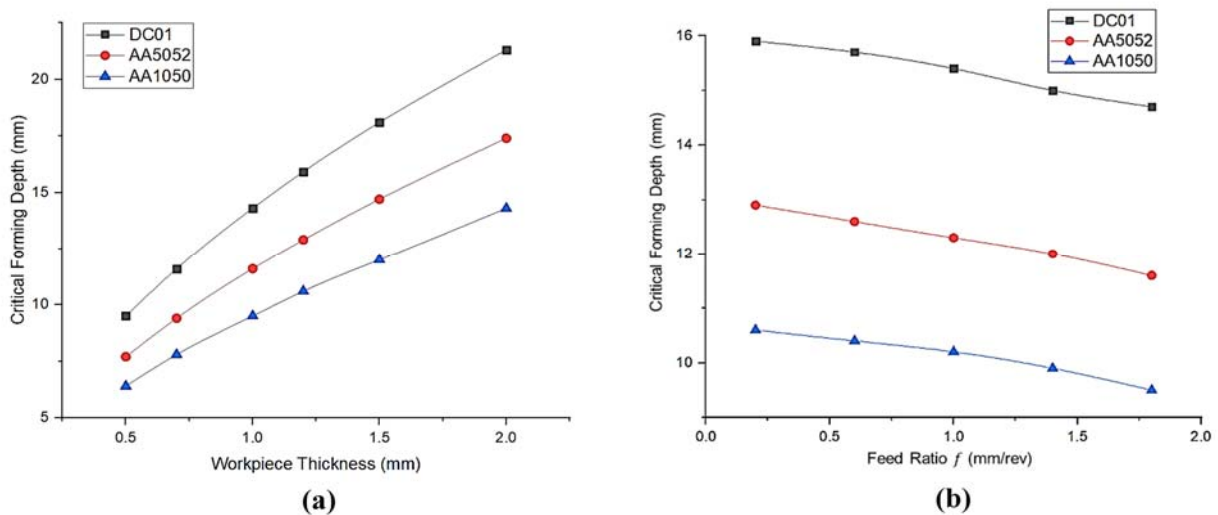
Fig. 10 Effect of blank thickness and feed ratio on wrinkling (R_O =50 mm, R_C =20 mm)
(a) critical forming depth vs. thickness; (b) critical forming depth vs. feed ratio (t = 1.2 mm).

5.2   Experimental Validation of Wrinkling Prediction Model

5.2.1 Experimental Design and Procedure

Experimental tests of the first-pass conventional spinning using convex, concave and linear toolpath profiles are conducted in order to validate the analytical wrinkling prediction model integrated with toolpath design. The D-optimal Design of Experiment has generated the experimental test runs of the combination of variation levels of the process parameters as shown in Table 1 and Figure 7. Using the blank diameter of 75 mm and the spin ratio of 0.73, the first 13 experimental test runs investigate the effect of blank thickness, feed ratio and the toolpath profiles of $-2\lambda, 0, +2\lambda$ defining convex, linear and concave path curvature respectively. To evaluate the effect of a varied spin ratio, additional five experimental test runs of No. 14-18 are designed in Table 1. All testing blanks are made of mild steel (DC01) and the clamping radius R_C is kept constant as 20 mm for all experimental test runs.
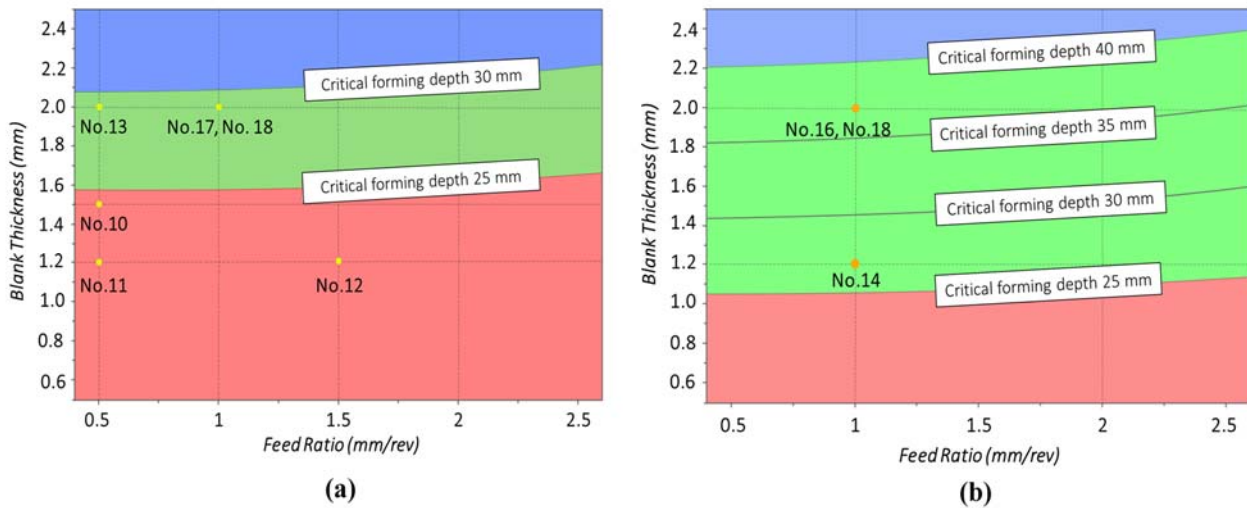
Fig. 11 Predicted critical forming depths using concave toolpath +2λ: (a) spin ratio 0.73; (b) spin ratio 0.80.

By applying the analytical wrinkling prediction model using a concave toolpath profile with path curvature +2λ, for the blank thickness varying from 0.5 to 2.5 mm and feed ratio varying from 0.4 to 2.6 mm/rev, the contour lines of the critical forming depth is predicted for spin ratio of 0.73 and 0.80 respectively, as shown in Figure 11. For each test, the specific critical forming depth of test runs, No. 10-18 using the concave toolpath +2λ, is highlighted on the contour lines. For example, for test run No.13 using blank thickness of 2 mm, feed ratio of 0.5 mm/rev, the predicted critical forming depth at the onset of the wrinkling is between 25~30 mm and if the forming depth applied in test run No. 13 is below 25 mm, wrinkling should not occur.

The "Predicted critical forming depth" for each test run is presented in Table 1. By considering the predicted critical forming depths, two values of 25 mm and 40 mm are employed in the test runs and the "Applied forming depth" for each test is shown in Table 1. As discussed in Section 2, a concave toolpath is considered as the worst case for wrinkling in designing toolpaths. If the wrinkling is avoided by employing the concave path curvature +2λ in test runs No.10-13, then applying the convex path curvature −2λ and linear path curvature 0 with the same applied forming depth of 25 mm, test runs No.1-9 should produce wrinkle-free parts. By comparing the corresponding forming depth obtained in the experiment with that predicted from the analytical model, the actual test results of wrinkled and wrinkle-free spun parts provide a validation of the wrinkling prediction model. To ensure repeatability of the experimental results, each test run is performed twice. The measurement results of the vibration waveforms are evaluated to determine if wrinkling has occurred in cases of minor winkles. If there is any discrepancy between the results of two test runs using the same process parameters, a third test is performed to confirm if wrinkling has occurred or not.

5.2.2 Experimental Validation Results

The spun parts produced in the experimental tests of the first-pass conventional spinning are shown in Figure 12. The time-domain vibration signals for each test during the whole duration of the spinning process is obtained and examined. When producing a wrinkle-free spun part, it is observed that the fluctuation of the vibration amplitude during spinning is in the range of ±10mV. As shown in Figure 13, two examples of wrinkle-free spinning tests, No.1 and No.13, show that the majority of the vibration

amplitude varies within this range. Thus the variation range of the vibration amplitude greater than ±10mV is used as limits to detect the initiation of wrinkling in the experiment.
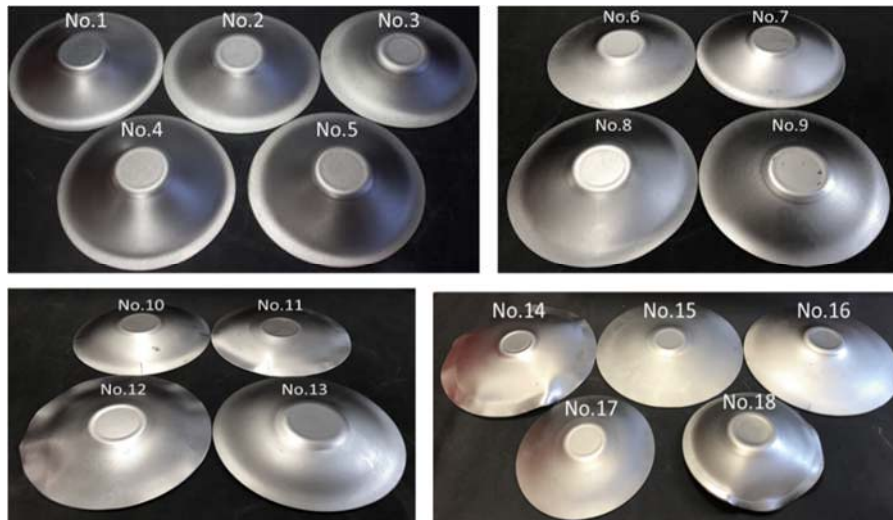
Fig. 12 Experimental spun parts of test runs No.1-18
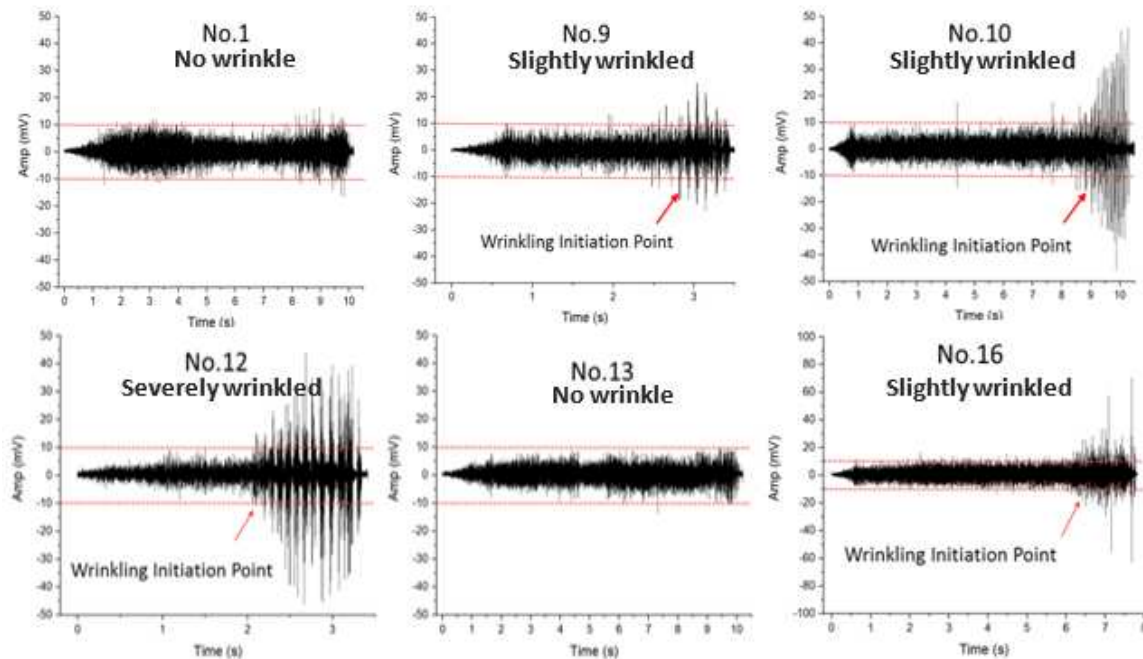
Fig. 13 Time-domain vibration measurements to detect wrinkle initiation
(No.1 – Convex toolpath; No.9 – Linear toolpath; No.10, 12, 13 and 16 – Concave toolpath).

For the first thirteen test runs, wrinkles can be observed clearly on the spun parts of tests No.11 and 12, while no visible wrinkles can be observed on the other spun parts. However, by evaluating the time-domain vibration measurement results, the variation of the vibration amplitude for selected tests in Figure 13 have shown that minor wrinkles are generated in test runs No.9 and 10. For the last five test runs, wrinkling has occurred in No.14, 16 and 18 as shown in Figures 12 and 13. From the wrinkling results in test runs No.10-18, it is clear the wrinkling has occurred if the applied forming depth, h, is greater than the predicted critical forming depth, h_c, as shown in Table 1. For example, for test runs No.14-16 using a higher spin ratio of 0.8, if a higher forming depth of 40 mm, greater than the predicted critical forming depths, is applied, the wrinkling has occurred, as shown in Figure 12.

Comparing the wrinkling results obtained from test runs No.1-8 with that from test runs No.10-12, it is also clear that applying the convex and linear toolpath profiles have avoided wrinkling by using the applied forming depth of 25 mm; however, employing the concave toolpath of the same applied forming depth has resulted in wrinkling. The experimental wrinkling results have confirmed the assumption that the concave toolpath profile is the worst case in toolpath design, as discussed in Section 2. This is in agreement with that reported by Hayama et al. (1970) and Watson et al. (2015).

Table 1 Experimental test runs, parameters and test results of wrinkling for validation

Test run	Blank thickness t (mm)	Feed ratio f (rev/mm)	Path curvature	Spin ratio τ	Predicted critical forming depth, h_c (mm)	Applied forming depth, h (mm)	Test result
No.1	1.2	0.5	-2λ (convex toolpath)	0.73	At least 25	25	No wrinkle
No.2	2	1					No wrinkle
No.3	2	1.5					No wrinkle
No.4	1.5	0.5					No wrinkle
No.5	1.5	1					No wrinkle
No.6	2	1.5	0 (linear toolpath)	0.73	At least 25	25	No wrinkle
No.7	1.2	0.5					No wrinkle
No.8	1.2	1					No wrinkle
No.9	1.5	1.5					Wrinkled
No.10	1.5	0.5	$+2\lambda$ (concave toolpath)	0.73	< 25	$25 > h_c$	Wrinkled
No.11	1.2	0.5		0.73	< 25	$25 > h_c$	Wrinkled
No.12	1.2	1.5		0.73	< 25	$25 > h_c$	Wrinkled
No.13	2	0.5		0.73	$25 \sim 30$	$25 = h_c$	No wrinkle
No.14	1.2	1	$+2\lambda$ (concave toolpath)	0.8	$25 \sim 30$	$40 > h_c$	Wrinkled
No.15	2	1		0.8	$35 \sim 40$	$25 < h_c$	No wrinkle
No.16	2	1		0.8	$35 \sim 40$	$40 > h_c$	Wrinkled
No.17	2	1	$+2\lambda$ (concave)	0.73	$25 \sim 30$	$25 < h_c$	No wrinkle
No.18	2	1		0.73	$25 \sim 30$	$40 > h_c$	Wrinkled

The critical forming depth obtained from the wrinkling prediction model under various spinning conditions is generally greater than that can be applied in the experimental tests to avoid wrinkling. It means that the prediction is more conservative than that observed in the experimental tests, i.e. a slightly higher forming depth could be applied in the experiment but still avoids wrinkling in the final spun part. This is in agreement with experimental observations that minor wrinkles occurring during an early stage in spinning may be smoothed out by the subsequent blank deformation by the roller tool. Another explanation is that the circumferential compressive force may be reduced by frictional force at the tool and blank contact interface, because the direction of the frictional force is opposite to the rolling

direction of the tool circumferentially. However, in the analytical prediction model, the effect of friction is neglected, resulting in a greater circumferential tool force and the external work done to produce a conservative prediction of the onset of wrinkling than that observed in the experiment tests.

5.3 Processing Maps for Wrinkle-free Conventional Spinning

Having experimentally validated the wrinkling prediction model for the first-pass conventional spinning, a regression analysis of the predicted results is firstly performed to evaluate the statistically significant spinning parameters. Finally, processing maps are created for wrinkling free conventional spinning processes.

Table 2 Analytical test runs, parameters and wrinkling prediction for significance analysis

Test No.	Thickness t (mm)	Feed Ratio f (mm/rev)	Spin Ratio τ	Predicted critical forming depth, h_c (mm	Wrinkling Sensitivity η
1	1	0.5	0.3	6.89	1.306
2	1.5	0.5	0.5	14.18	1.481
3	2	0.5	0.3	9.53	0.944
4	1	0.5	0.7	18.67	2.624
5	1.5	0.5	0.7	23.6	2.076
6	2	1	0.7	27.11	1.807
7	1	1	0.5	11.29	1.860
8	1.5	1	0.5	13.68	1.535
9	2	1	0.3	9.32	0.966
10	1	2	0.3	6.49	1.387
11	1.5	2	0.3	8.44	1.066
12	2	2	0.5	15.51	1.354
13	1	2	0.7	17.34	2.826

From the experimental wrinkling results, it is clear that the blank thickness, feed ratio and spin ratio affect the onset of the wrinkling. To evaluate the significance of each of these parameters, a design of analytical tests using the Box-Behnken Design of Experiments is created where spin ratio of 0.3, 0.5 and 0.7, blank thickness of 1, 1.5 and 2 mm, and feed ratio of 0.5, 1 and 2 mm/rev are applied, as shown in Table 2. The critical forming depth is obtained by using the analytical wrinkling prediction model and the wrinkling sensitivity is calculated, as presented in Table 2. The critical forming depth and wrinkling sensitivity are selected as two responses of statistical analysis. Each data set is fitted to form a multiple linear regression (MLR) model and the coefficient of the regression analysis is used to determine the significance of each of the spinning parameters on each of the responses, i.e. the critical forming depth and wrinkling sensitivity, respectively. In order to identify the most significant effects of the spinning parameters and their interactions on wrinkling, only linear and square terms in each of the MLR models are considered. Figure 14 shows the significance analysis results for both responses with an error bar indicating the 95% confidence interval. Both graphs show that the most significant parameter affecting wrinkling is the spin ratio, followed by the blank thickness, the spin ratio-blank thickness interaction. However, for the spinning conditions tested, the feed ratio (varying from 0.5

mm/rev to 2 mm/rev), spin ratio-feed ratio interaction and thickness-feed ratio interaction have relatively less significance.
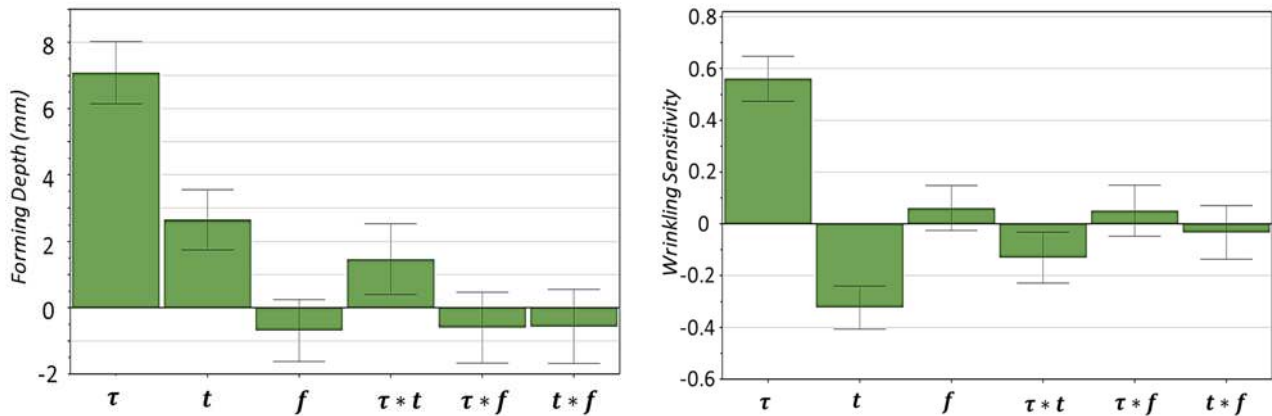
Fig. 14 Significance of main spinning parameters on critical forming depth and wrinkling sensitivity
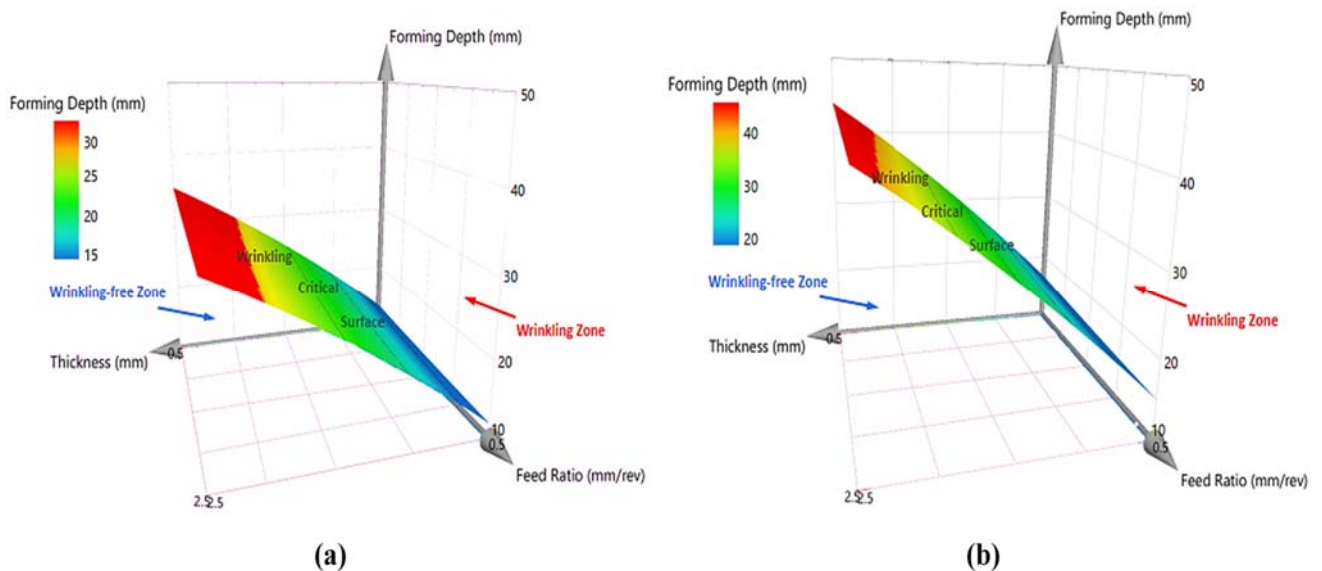
Fig. 15 Processing maps to predict wrinkling at different spin ratios (a) $\lambda=0.73$ (b) $\lambda=0.80$

After evaluating the significance of the main spinning process parameters, three-dimensional processing maps are produced by varying feed ratio, blank thickness and spin ratio to predict the critical forming depth to separate the safe and wrinkling regions in the first-pass conventional spinning, as shown in Figure 15. The wrinkling critical surface shown in the processing map indicates the critical forming limit under different values of blank thickness, feed ratio and spin ratio. The wrinkling critical surface separates the wrinkle-free zone and wrinkling zone when the main spinning process parameters vary over the selected ranges of these main parameters. The processing map can therefore be utilised to select the spinning process parameters for practical applications. If the proposed process parameters in any spinning process are located within the wrinkling zone according to the processing map, wrinkling is predicted to occur during the spinning process, suggesting that the spinning parameters must be changed to avoid the onset of the wrinkling.

6   Conclusions

An analytical model integrated with toolpath design is developed in this study to predict the onset of wrinkling in first-pass conventional spinning. The prediction results are validated by the experiment using concave, convex and linear toolpath profiles under varied ranges of important spinning process parameters, including blank thickness, feed ratio and spin ratio. The following conclusions may be drawn:

1) The cubic Bézier curve is effective in designing various toolpath profiles including concave, convex and linear paths where the path curvature can be flexibly specified;

2) The critical forming depth is proposed for the first time in this study as a critical variable in designing each toolpath profile for multi-pass conventional spinning. Both the analytical prediction and experimental results have shown it is an accurate and effective measure in predicting the onset of the wrinkling;

3) The spin ratio is introduced by defining the ratio of the un-supported flange dimension of the blank to the original radius of the blank. It enables the effect of blank dimension and clamped area during spinning on the onset of wrinkling to be evaluated;

4) Under the same spinning conditions and applying the same forming depth, employing a convex or linear toolpath profile lead to wrinkle-free spinning, however using a concave toolpath profile results in wrinkling;

5) The significance analysis of the spinning process parameters shows that the most important parameter affecting the wrinkling is the spin ratio, followed by the blank thickness, the spin ratio-blank thickness interaction. For the variation range of the feed ratio tested, varying from 0.5 mm/rev to 2 mm/rev, the significance of the feed ratio and its interaction with other main parameters is less strong;

6) Three-dimensional process maps are produced to predict wrinkle-free and wrinkling zones in the first-pass conventional spinning. It can be used as a tool in designing toolpath profiles and selecting key spinning process parameters in practical applications.

References:
Chen, S. W., Gao, P. F., Zhan, M., Ma, F., Zhang, H. R., Xu, R. Q., 2019. Determination of formability considering wrinkling defect in first-pass conventional spinning with linear roller path. Journal of Materials Processing Technology, 265, 44–55.

Chen, S. W., Zhan, M., Gao, P. F., Ma, F., Zhang, H. R., 2021. A new robust theoretical prediction model for flange wrinkling in conventional spinning. Journal of Materials Processing Technology, 288, 116849.

Childerhouse, T., Long, H., 2019. Processing maps for wrinkle free and quality enhanced parts by shear spinning. Procedia Manufacturing, 29, 137-144.

Essa, K., Hartley, P., 2010. Optimization of conventional spinning process parameters by means of numerical simulation and statistical analysis. Proceedings of the Institution of Mechanical Engineers, Part B: Journal of Engineering Manufacture, 224(11), 1691–1705.

Gan, T., Kong, Q., Yu, Z., Zhao, Y., Lai, X., 2016. A numerical study of multi-pass design based on Bezier curve in conventional spinning of spherical components. MATEC Web of Conferences, 2016 volume 80.

Hayama, M., Tago, K., 1968. The fracture of walls on shear spinning: study on the spin ability of aluminium plates. Bulletin of the Faculty of Engineering, Yokohama National University, 17, 93–103.

Hayama, M., Kudo, H., Shinokura, T., 1970. Study of the pass schedule in conventional simple spinning. Bulletin of JSME, 13(65), 1358–1365.

Hayama, M., 1981 Study on spin ability of aluminium and its alloys. Bulletin Faculty Engineering Yokohama National University, 30, 63–72.

Kawai, K., Hayama, M., 1987. Roller pass programming in conventional spinning by NC spinning machine. Advanced Technology of Plasticity 1987, edt. by Lange, K., 2, 711-718, Springer-Verlag.

Hosford, W. F., Duncan, J. L., 1999. Sheet metal forming: A review. JoM, the Journal of the Minerals, Metals & Materials Society, 51(11), 39-44.

Hutchinson, J.W., Neale, K.W., 1985. Wrinkling of curved thin sheet metal. Plastic Instability, Considère Mémorial Symposium, 71-78, Presses Ponts et Chaussées, Paris.

Kegg, R. L., 1961. A New Test Method for Determination of Spin ability of Metals. Trans. ASME, series B, Journal of Engineering for Industry, 83(B), 119–124.

Kleiner, M., Gobel, R., Kantz, H., Klimmek, C., Homberg, W., 2002. Combined Methods for the Prediction of Dynamic Instabilities in Sheet Metal Spinning. CIRP Annals - Manufacturing Technology, 51(1), 209–214.

Kobayashi, S., 1963. Instability in conventional spinning of cones. Transactions of the ASME, Journal of Engineering for Industry, 85, 44–48.

Kong, Q., Yu, Z., Zhao, Y., Wang, H., Lin, Z., 2017. Theoretical prediction of flange wrinkling in first-pass conventional spinning of hemispherical part. Journal of Materials Processing Technology, 246, 56–68.

Li, Y., Wang, J., Lu, G. D., Pan, G. J., 2014. A numerical study of the effects of roller paths on dimensional precision in die-less spinning of sheet metal. J. of Zhejiang University: Science A., 15(6), 432–446.

Liu, J. H., Yang, H., Li, Y. Q., 2002. A study of the stress and strain distributions of first-pass conventional spinning under different roller-traces. Journal of Materials Processing Technology, 129(1), 326–329.

Marciniak, Z., Duncan, J.L., Hu, S.J., Mechanics of Sheet Metal Forming. Second edition, Butterworth-Heinemann, 2002.

Music, O., Allwood, J. M., Kawai, K., 2010. A review of the mechanics of metal spinning. Journal of Materials Processing Technology, 210(1), 3–23.

Novozhilov, V. V., Thin Shell Theory. Ed., 2nd r. Groningen: Groningen: P. Noordhoff, 1964.

Shim M. S., Park, J. J., 2001. The formability of aluminium sheet in incremental forming. Journal of Materials Processing Technology, 113(1), 654–658.

Polyblank, J. A., Allwood, J. M., 2015. Parametric toolpath design in metal spinning. CIRP Annals - Manufacturing Technology, 64(1), 301–304.

Runge, M., Spinning and Flow forming, (D.H. Pollitt, Trans) Leifield GmbH, Werkzeugmaschinenbau/Verlag Moderne Industrie AG, D-86895, Landsberg/Lech, 1994.

Sebastiani, G., Brosius, A., Ewers, R., Kleiner, M., Klimmek, C., 2006. Numerical investigation on dynamic effects during sheet metal spinning by explicit finite-element-analysis. Journal of Materials Processing Technology, 177(1), 401–403.

Senior, B.W., 1956. Flange wrinkling in deep-drawing operations. Journal of the Mechanics and Physics of Solids, 4, 235–246.

Timoshenko, S. P., Woinowsky-Krieger, S., Theory of Plates and Shells. Second Ed. New York: McGraw-Hill, 1959.

Timoshenko, S. P., Gere, J. M. Theory of Elastic Stability. Second Ed. New York: McGraw-Hill, 1961.

Tomita, Y., 1994. Simulations of plastic instabilities in solid mechanics. Appl. Mech. Rev. 47(6), 171–205.

Tugcu, P., Neale, K.W., Wu, P.D., MacEwen, S.R., 2001. Effect of planar anisotropy on wrinkle formation tendencies in curved sheets. International Journal of Mechanical Sciences 43, 2883–2897.

Wang, L., Long, H., Ashley, D., Roberts, M., White, P., 2011. Effects of the roller feed ratio on wrinkling failure in conventional spinning of a cylindrical cup. Proceedings of the Institution of Mechanical Engineers, Part B: Journal of Engineering Manufacture, 225(11), 1991–2006.

Wang, L., Long, H., 2013. Roller path design by tool compensation in multi-pass conventional spinning. Materials and Design, 46, 645–653.

Wang, X., Cao, J., 2000. An analytical model for flange wrinkling in Sheet Metal Forming. Journal of Manufacturing Processes, 2(2), 100–107.

Wang, X., Cao, J., Li, M., 2001. Wrinkling analysis in shrink flanging, ASME J. Manuf. Sci. Eng., 123, 426–432.

Watson, M., Long, H., Lu, B., 2015. Investigation of wrinkling failure mechanics in metal spinning by Box-Behnken design of experiments using finite element method. International Journal of Advanced Manufacturing Technology, 78, 981-995

Wong, C. C., Dean, T. A., Lin, J, 2003. A review of spinning, shear forming and flow forming processes. International Journal of Machine Tools and Manufacture, 43(14), 1419–1435.

Xia, Q. X., Shima, S., Kotera, H., Yasuhuku, D., 2005. A study of the one-path deep drawing spinning of cups. Journal of Materials Processing Technology, 159(3), 397–400.

Zhan, M., Yang, H., Zhang, J. H., Xu, Y. L., Ma, F., 2007. 3D FEM analysis of influence of roller feed rate on forming force and quality of cone spinning. Journal of Materials Processing Technology, 187, 486–491.

Appendix A: Expressions of Plastic Strains of the Middle Surface

For a spun part to wrinkle during the first-pass conventional spinning using a concave toolpath, the principal strains ε_θ and ε_φ, shear strain $\gamma_{\theta\varphi}$, the curvature changes κ_θ and κ_φ, and the twist χ of the deformed middle surface, can be derived by adopting the Donnell-Mushtari-Vlasov theory (Novozhilov, 1964), a simplified deformation theory for thin shells. The expressions are:

$$\varepsilon_\theta = \frac{w}{r_1} \tag{Eq. A1}$$

$$\varepsilon_\varphi = \frac{w}{r} \tag{Eq. A2}$$

$$\gamma_{\theta\varphi} = 0 \tag{Eq. A3}$$

$$\kappa_\theta = -\frac{1}{r_1^2}\frac{\partial^2 w}{\partial\theta^2} - \frac{cos(\varphi_C + \varphi)}{rr_1}\frac{\partial w}{\partial\varphi} - \frac{w}{r_1^2} \tag{Eq. A4}$$

$$\kappa_\varphi = -\frac{1}{r^2}\frac{\partial^2 w}{\partial\varphi^2} - \frac{w}{r^2} \tag{Eq. A5}$$

$$\chi = -\frac{1}{rr_1}\frac{\partial^2 w}{\partial\theta\partial\varphi} + \frac{cos(\varphi_C + \varphi)}{r_1^2}\frac{\partial w}{\partial\theta} \tag{Eq. A6}$$

where $w\,(r,\theta,\varphi)$ is the displacement normal to the middle surface of the spun part in the z direction as shown in Figure 4a. r_1 and r are the principal radii along the circumferential direction and the meridional direction of the middle surface, respectively; θ and φ are the circumferential angle and the meridional angle of the middle surface, respectively. φc is the angle defining the blank clamping end point in the meridional direction of the middle surface.

Appendix B: Derivations of the Strain Energy of the Deformed Blank in Spinning

The generalised expression of the strain energy can be found in the Thin Shell Theory, Timoshenko and Woinowsky-Krieger (1959) and Novozhilov (1964). Based on the analysis of the blank deformation as described in Section 4.1, the strain energy of the deformed blank in spinning can be expressed by the strain components given in Equation 5 and Equations A1-A6:

$$U = \frac{t}{2}\iint \frac{E_s}{1-v^2}\left((\varepsilon_\theta+\varepsilon_\varphi)^2 + 2(1-v)\left(\frac{1}{4}\gamma_{\theta\varphi}-\varepsilon_\theta\varepsilon_\varphi\right)\right)rr_1d\theta d\varphi$$

$$+\frac{t^3}{24}\iint \frac{E_r}{1-v^2}\left((\kappa_\theta+\kappa_\varphi)^2 + 2(1-v)(\chi^2-\kappa_\theta\kappa_\varphi)\right)rr_1d\theta d\varphi \qquad \textbf{(Eq. B1)}$$

where t is the thickness of the blank; E_s, E_r, v are the secant modulus, reduced modulus, and Poisson's ratio of the blank material respectively. $\varepsilon_\theta, \varepsilon_\varphi, \gamma_{\theta\varphi}$ are the principal and shear strains; $\kappa_\theta, \kappa_\varphi, \chi$ are the curvature changes and the twist of the middle surface of the deformed blank, respectively.

By replacing the strain components as given in Equations A1-A6, and using the geometrical parameters of the deformed blank as illustrated in Figure 6:

$$U = \frac{tE_s}{2(1-v^2)}\iint \left(\frac{r}{r_1}+\frac{r_1}{r}+2v\right)w^2 d\theta d\varphi$$

$$+\frac{t^3E_r}{24\,(1-v^2)}\iint \left[\left(\frac{r}{r_1}\right)^2\left(\frac{\partial^2 w}{\partial\theta^2}+\frac{r_1}{r}cos(\varphi_c+\varphi)\frac{\partial w}{\partial\varphi}+\text{w}\right)^2 + \left(\frac{r_1}{r}\right)^2\left(\frac{\partial^2 w}{\partial\varphi^2}+\text{w}\right)^2\right.$$

$$+2v\left(\frac{\partial^2 w}{\partial\theta^2}+\frac{r_1}{r}cos(\varphi_c+\varphi)\frac{\partial w}{\partial\varphi}+\text{w}\right)\left(\frac{\partial^2 w}{\partial\varphi^2}+\text{w}\right)$$

$$\left.+2(1-v)\left(\frac{\partial^2 w}{\partial\theta\partial\varphi}-\frac{r}{r_1}cos(\varphi_c+\varphi)\frac{\partial w}{\partial\theta}\right)^2\right]d\theta d\varphi \qquad \textbf{(Eq. B2)}$$

By further replacing the wrinkling wave function given in Equation 2, the strain energy required for the blank to wrinkle, U, can be derived as

$$U = s^2\left(A_1m^4 + A_2m^2 + A_3\right) = 4\,R_2(R_0-R_2)\left(A_1m^2+A_2+\frac{A_3}{m^2}\right) \qquad \textbf{(Eq. 12)}$$

where m is the number of wrinkles (Equation 1); s is the wrinkle-wave amplitude (Equation 4); R_0 is the original radius of the blank; R_2 is the radius of the blank after first-pass of spinning, $R_2 = r\sin(\varphi_C+\varphi_i)$. The parameters, A_1, A_2, and A_3 in Equation 12, to calculate the strain energy of the wrinkled spun part, can be expressed as:

$$A_1 = -\frac{\pi t^3 E_r}{48(1-v^2)}\int_0^{\varphi_i}\frac{r}{r_1^3}\left[cos\left(\frac{\pi\varphi}{\varphi_i}\right)-1\right]d\varphi \qquad \textbf{(Eq. B3)}$$

Journal of Materials Processing Tech.

$$A_2 = -\frac{t^3 E_r}{24(1-v^2)}\int_0^{\varphi_i}\left[\frac{\pi^2(3-2v)sin\left(\frac{\pi\varphi}{\varphi_i}\right)cos(\varphi_c+\varphi)}{2r_1^2\varphi_i}\right.$$

$$+\frac{\pi r\left(cos\left(\frac{\pi\varphi}{\varphi_i}\right)-1\right)\left(1-(1-v)cos^2(\varphi_c+\varphi)\right)}{r_1^3} + \frac{v\pi\left(cos\left(\frac{\pi\varphi}{\varphi_i}\right)-1\right)}{r_1 r}$$

$$\left.+\frac{\pi^3\left[2(1-v)cos^2\left(\frac{\pi\varphi}{2\varphi_i}\right)-\left(cos\left(\frac{\pi\varphi}{\varphi_i}\right)-1\right)\right]}{4r_1 r\varphi_i^2}\right]d\varphi \qquad (\text{Eq. B4})$$

$$A_3 = \frac{t^3 E_r}{24(1-v^2)}\int_0^{\varphi_i}\left[\frac{3\pi^3 cos^2\left(\frac{\pi\varphi}{2\varphi_i}\right)cos^2(\varphi_c+\varphi)+3\pi\left(cos\left(\frac{\pi\varphi}{\varphi_i}\right)-1\right)+3\pi^2 v\left(cos\left(\frac{\pi\varphi}{\varphi_i}\right)-1\right)}{4r_1 r\varphi_i^2}\right.$$

$$+\frac{3\pi^2 sin\left(\frac{\pi\varphi}{2\varphi_i}\right)cos(\varphi_c+\varphi)}{2r_1^2\varphi_i}-\frac{3\pi r\left(cos\left(\frac{\pi\varphi}{\varphi_i}\right)-1\right)}{2r_1^3}-\frac{3\pi^5 r\left(cos\left(\frac{\pi\varphi}{\varphi_i}\right)-1\right)}{32r_1^3\varphi_i^4}$$

$$-\frac{3\pi\left(cos\left(\frac{\pi\varphi}{\varphi_i}\right)-1\right)}{2r^2}-\frac{3\pi^4 v sin\left(\frac{\pi\varphi}{\varphi_i}\right)cos(\varphi_c+\varphi)}{8r^2\varphi_i^3}+\frac{3\pi^2 v sin\left(\frac{\pi\varphi}{\varphi_i}\right)cos(\varphi_c+\varphi)}{2r^2\varphi_i}$$

$$\left.-\frac{3\pi v\left(cos\left(\frac{\pi\varphi}{\varphi_i}\right)-1\right)}{r_1 r}\right]d\varphi+\frac{3\pi t E_s}{2(1-v^2)}\int_0^{\varphi_i}\left[\left(\frac{r}{r_1}+\frac{r_1}{r}+2v\right)sin^2\left(\frac{\pi\varphi}{2\varphi_i}\right)\right]d\varphi \quad (\text{Eq. B5})$$

where r_1 and r are the principal radii along the circumferential direction and the meridional direction of the middle surface, respectively; θ and φ are the circumferential angle and the meridional angle of the middle surface, respectively. φ_C is the angle defining the blank clamping end point and φ_i is the subtending angle of the concave toolpath profile in the meridional direction of the middle surface.